Trans. Japan Soc. Aero. Space Sci.
Vol. 63, No. 2, pp. 62–65, 2020
DOI: 10.2322/tjsass.63.62

Research Note

Optimal Endurance and Range of Electric Aircraft with Battery Degradation*

Sung Wook PAEK,[1)†] Sangtae KIM,[2)] and Rayappan Vinoth RAJ[1)]

[1)]*Materials R&D Center, Samsung SDI, Gyeonggi-do 16678, Republic of Korea*
[2)]*Center for Electronic Materials, Korea Institute of Science and Technology, Seoul 02792, Republic of Korea*

Key Words: Electric Aircraft, Battery, Flight Dynamics, Simulation, Optimization

Nomenclature

$C_{D,0}$: parasitic drag coefficient
D: drag, N
I: current, A
K: induced drag coefficient
L: lift, N
n: number of cycles used
P: power, W
Q: electric charge, C
S: wing area, m^2
T: thrust, N
t: time, s
U: battery terminal voltage, V
v: velocity, m/s
x: horizontal position, m
α, β: degradation coefficients

Subscripts

0: initial
1C: 1 C-rated
E: endurance
f: final
R: range

Superscripts

*: optimal
˙: time derivative

1. Introduction

Electric aircraft is a promising candidate to provide on-demand air mobility in future transportation.[1,2)] Although the performance of battery-powered electric aircraft is highly dependent on battery performance, little has been known regarding their relationship, especially in the long term.[3)] Traub investigated the optimal range and endurance of electric aircraft utilizing lead-acid batteries,[4)] while Kaptsov analyzed the same with Li-ion batteries (LIBs).[5,6)] The scope of these papers was limited to the beginning of life (BOL) performance of batteries. However, LIBs exhibit intriguing degradation patterns over their life when used in IT devices or electric vehicles; first, the formation of stable solid-electrolyte interphase (SEI) layers in LIBs can slow down degradation,[7)] unlike other kinds of batteries (e.g., fuel cell).[8)] Towards the end of life (EOL), on the other hand, unfavorable usage conditions may cause lithium decomposition in the LIB anode and exponentially accelerate capacity degradation.[9)] This paper considers several LIB degradation scenarios and compares their influence on the long-term performance of battery-powered electric aircraft. The designer, the manufacturer, and the operator of electric aircraft would thereby know which battery gives the most number of cycles under various mission scenarios.

The organization of the rest of this paper is as follows. Flight dynamics of electric aircraft is discussed in Section 2. Representative battery aging scenarios are described in Section 3, followed by case studies in Section 4. Lastly, conclusions are drawn in Section 5.

2. Flight Dynamics of Electric Aircraft

For an aircraft to cruise steadily at a constant altitude, forces must be balanced in vertical and horizontal directions:

$$\dot{x} = v, \quad \dot{v} = 0, \quad L = W, \quad T = D, \tag{1}$$

where the total drag (D) above consists of two terms[10)]

$$D = \frac{1}{2} C_{D,0} \rho S v^2 + \frac{2KW^2}{\rho S v^2}. \tag{2}$$

The former term (parasitic drag) is proportional to the squares of airspeed, and the latter (lift-induced drag) is inversely proportional to the squares of airspeed. The net power required is the product of this drag and velocity by Eqs. (1) and (2)

$$P = Tv = Dv = \eta P_e = \eta U I = -\eta U \dot{Q}. \tag{3}$$

In Eq. (3), power is also equal to the product of electric power (P_e) and system efficiency. The electric power is obtained by multiplying voltage (U) and current (I). Current is the negative of the time derivative of electric charge, whose overall sign is positive during discharge with the battery charge decreasing ($\dot{Q} < 0$). Combining Eq. (2) and Eq. (3) gives

$$\dot{Q} = -\frac{Tv}{\eta U} = -\frac{Dv}{\eta U} = -\frac{C_{D,0}\rho^2 S^2 v^4 + 4KW^2}{2\rho S v^2 \eta U_{nom}}, \tag{4}$$

where the current draw is a function of aircraft design parameters and battery parameters, as summarized in Table 1 and Table 2.[5)] These numbers closely reflect Airbus Group's E-

*Received 2 October 2018; final revision received 30 August 2019; accepted for publication 10 October 2019.
†Corresponding author, pswpsh@gmail.com

Table 1. Aircraft design parameters.

Parameter	Value
Max takeoff weight (W)	600 kgf
Wing area (S)	10 m^2
Thrust (T)	1500 N
Air density (ρ)	1.1 kg/m^3
Total system efficiency (η)	0.68
Parasitic drag coefficient ($C_{D,0}$)	0.025
Induced drag coefficient (K)	0.039

Table 2. Battery parameters.

Parameter	Value
Initial charge (Q)	288000 C (80 Ah)
System voltage	250 V
70% life	10000 cycles

Fan, which is the first all-electric, battery-powered two-seater plane with twin ducted fan motors. The dimensions and propulsion parameters are obtained from the manufacturer's design specifications, and the aerodynamic parameters have been shown to match the aircraft performance.

Kaptsov formulated an optimal control problem for electric aircraft to maximize range and endurance using Pontryagin's minimum principle.[6] The same results are derived here via simple calculus in flight dynamics. First, endurance is given by $Q/|\dot{Q}|$ where $|\dot{Q}|$ is proportional to Dv. To maximize endurance, therefore, Dv should be minimized by

$$\frac{\partial(Dv)}{\partial v} = \frac{\partial}{\partial v}\left[\frac{1}{2}C_{D,0}\rho S v^3 + \frac{2KW^2}{\rho S v}\right] = 0, \tag{5}$$

from which the endurance-optimal cruise velocity v_E^* is

$$v_E^* = \sqrt{\frac{2W}{\rho S}\sqrt{\frac{K}{3C_{D,0}}}}, \tag{6}$$

and the corresponding maximum endurance E^* is

$$E^* = \frac{Q_0}{|\dot{Q}|^*} = \frac{Q_0\eta U_{nom}}{D^* v_E^*} = \frac{3^{3/4}\eta U_{nom} Q_0\sqrt{\rho S}}{2^{5/2}C_{D,0}^{1/4}K^{3/4}W^{3/2}}. \tag{7}$$

Similarly, range is given by $vQ/|\dot{Q}|$ where $|\dot{Q}|/v$ is proportional to D which should be minimized for maximum range

$$\frac{\partial D}{\partial v} = \frac{\partial}{\partial v}\left[\frac{1}{2}C_{D,0}\rho S v^2 + \frac{2KW^2}{\rho S v^2}\right] = 0, \tag{8}$$

with the range-optimal velocity

$$v_R^* = \sqrt{\frac{2W}{\rho S}\sqrt{\frac{K}{C_{D,0}}}}, \tag{9}$$

and the corresponding optimal range

$$R^* = v_R^* t_R = \frac{Q_0\eta U_{nom}}{D} = \frac{Q_0\eta U_{nom}}{2\,W\sqrt{C_{D,0}K}}. \tag{10}$$

Note that the effect of battery degradation has not been included yet, leaving a question whether v_R^* and v_E^* are only optimal for factory-new batteries. As it will turn out, v_R^* is no longer optimal under battery degradation; v_R^* is affected by the shape of degradation curves over a battery's life.

3. LIB Degradation Scenarios

The battery life is defined as the time required for fully charged capacity to reach a certain threshold, 80% for example. Throughout its life, a LIB may exhibit diverse degradation patterns. The first scenario has a linear capacity fade without changes in slope (dQ/dt)[11]:

$$Q_1(n) = Q_0(1 - \alpha_1 n). \tag{11}$$

The second scenario assumes that capacity degradation is proportional to the square root of time. This relationship is derived from the loss of lithium ions which are irreversibly spent during the formation of SEI layers.[12] The elapsed time t is replaced with the cycle number n for discretization purposes and per industrial practices here:

$$Q_2(n) = Q_0(1 - \alpha_2\sqrt{n}). \tag{12}$$

The third scenario incorporates an exponential decay to the square-root degradation mode.[12] If a battery is cycled with high currents or low ambient temperatures, lithium is irreversibly deposited at the surface of anode particles, creating dendrites.[13] The ions must pass through the unblocked regions which are becoming narrower over time, increasing local current density and expediting lithium deposition again.[14] The cascading effect is represented as an exponential term in

$$Q_3(n) = Q_0\left(1 - \alpha_3\sqrt{n} - \alpha_4 e^{n/\beta}\right). \tag{13}$$

Coefficients α_i in these equations depend on capacity-normalized current (C-rate), depth of discharge (DOD), and battery cell temperature. If α_i is a function of C-rate only,

$$\alpha_i = \alpha_{i,1C}\frac{I}{I_{1C}} = \alpha_{i,1C}\frac{|\dot{Q}|}{I_{1C}}. \tag{14}$$

The degradation slope increases proportionally if the current is n multiples of I_{1C} (nC). The denominator is the 1 C-baseline current (I_{1C}), 80 A for an 80 Ah pack (Table 2), which completely discharges the battery pack in an hour. As shown in Eq. (4), the discharge rate is a nonlinear function of cruise velocity. If updated every Δn cycles, the recursive form of battery capacity is

$$Q(n + \Delta n) = Q(n) - \Delta Q(n), \tag{15}$$

with scenario-wise decrements of

$$\Delta Q_1(n) = -\alpha_1 Q_0 \Delta n, \tag{16}$$

$$\Delta Q_2(n) = -\frac{\alpha_2}{2\sqrt{n}} Q_0 \Delta n, \tag{17}$$

$$\Delta Q_3(n) = -\frac{\alpha_3}{2\sqrt{n}} Q_0 \Delta n - \frac{\alpha_4}{\beta} Q_0 e^{n/\beta}\Delta n, \tag{18}$$

Table 3 summarizes the coefficient values in three scenarios which all have 80% SOH (EOL) at 7000 cycles (Fig. 1). Scenario 1 may best describe real degradation patterns if SEI effects are not dominant due to chemical compositions.

Table 3. Degradation curve parameters.

Parameter	Value	Scenario
α_1	2.86×10^{-5}	1
α_2	2.41×10^{-3}	2
α_3	2.00×10^{-3}	3
α_4	3.10×10^{-5}	3
β	1000	3

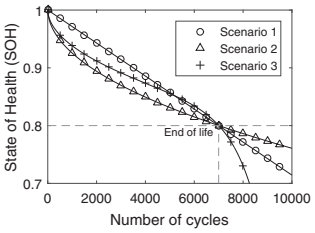

Fig. 1. Lithium-ion battery (LIB) degradation scenarios.

Whether a LIB will degrade like Scenario 2 or 3 depends on usage conditions and the robustness of a battery thereto. Although initially all matched-up, the endpoints of three scenarios at EOL are subject to change differently as the curves in Fig. 1 scale up or down horizontally in accordance with battery capacity and flight speed through Eqs. (4) and (14).

4. Optimal Cumulative Endurance and Range

The following procedures were taken to identify optimal cruise velocities in different scenarios. First, a cruise velocity was selected between 50 km/h to 150 km/h to calculate the discharge rate $\dot{Q}$ using Eq. (4), which was maintained at constant values until 80% SOH was reached using one of Eqs. (16), (17), and (18) depending on scenarios. Throughout battery life, endurance ($E = Q/\dot{Q}$) and range ($R = vQ/\dot{Q}$) were obtained in each cycle and then accumulated. Figure 2 depicts the variation of cumulative lifetime endurances with respect to cruise velocity in different battery degradation scenarios. The cumulative endurance is maximized at 99.8 km/h regardless of degradation patterns, equal to the optimal velocity without battery degradation given by Eq. (6). However, the order of total endurances is Scenario 2 (9347 h) > Scenario 1 (8408 h) > Scenario 3 (7797 h), different from the order of area under degradation curves in Fig. 1 (Scenario 1 > Scenario 3 > Scenario 2). This is because the battery's C-rate is not 1 C in this aircraft's design; the optimal velocity of 99.8 km/h actually corresponds to 0.88 C with 69.3 A from Eq. (4), stretching curves in Fig. 1 to the right in accordance with Eq. (14). If stretched, a scenario which is flatter in shape at the EOL would provide more cycles, as shown in Fig. 3(a): Scenario 2 (9331 cycles) > Scenario 1 (8807) > Scenario 3 (7547). The area order in Fig. 1 would have been preserved if the battery capacity had been around 69.3 Ah, as shown in Fig. 3(b) because all scenarios reach EOL at 7000 cycles as shown in Fig. 1: Scenario 1 (6300 h) > Scenario 3 (6198 h) > Scenario 2 (6078 h). The number of cycles (hours) has decreased because the battery capacity decreases from 80 Ah to 69.3 Ah.

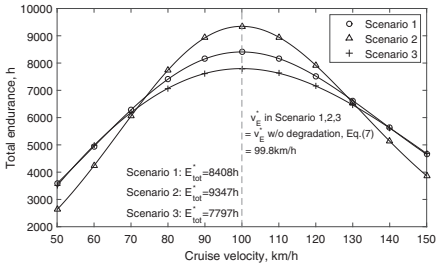

Fig. 2. Total endurances for battery degradation Scenarios 1, 2, and 3.

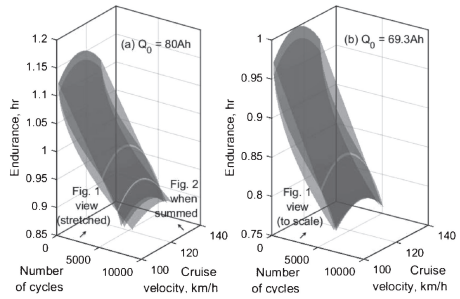

Fig. 3. Endurance history of Scenarios 1, 3, and 2 (top-down order) at (a) $Q_0 = 80$ Ah and (b) $Q_0 = 69.3$ Ah.

Similar phenomena are observed in cumulative lifetime ranges with an exception that optimal cruise velocities vary according to degradation scenarios. The total range follows an order of Scenario 2 (9.85×10^5 km) > Scenario 1 (9.07×10^5 km) > Scenario 3 (8.59×10^5 km), now achieved at different velocities of 111 km/h, 116 km/h, and 120 km/h, respectively, as shown in Fig. 4. This velocity difference is possibly explicable by the different goal of the range optimization relative to the endurance optimization problem; the latter aims to maximize flight time only, whereas range optimization maximizes the product of velocity and time, providing more degrees of freedom with respect to velocity choices. Scenario 2 achieves the longest range by opting for the smallest cruise velocity which stretches its EOL-flat curve and provides the highest number of battery cycles (flights). The order of total ranges is congruent with that of the number of cycles: Scenario 2 (9011 cycles) > Scenario 1 (7798) > Scenario 3 (7355). If the battery capacity is again reduced to 69.3 Ah, all scenarios reach EOL simultaneously and their ranges have the same order as areas in Fig. 1: Scenario 1 (6.80×10^5 km) > Scenario 3 (6.75×10^5 km) > Scenario 2 (6.40×10^5 km). Cycle-wise ranges at 80 Ah and 69.3 Ah are presented in Fig. 5(a) and Fig. 5(b), respectively.

Although this example gives useful insights, its mission profile is not realistic because (1) the battery is fully discharged, (2) the cruise velocity must be adjusted if different types of batteries are used, and (3) the flight distance decreases at every sortie (Fig. 5). Therefore, a practical mission resembling urban air mobility (UAM) operations is considered and briefly analyzed. First, battery discharging is main-

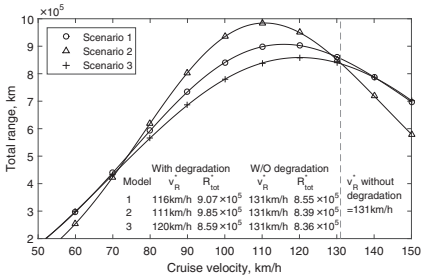

Fig. 4. Total ranges for battery degradation Scenarios 1, 2, and 3.

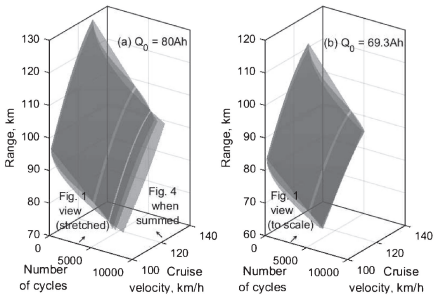

Fig. 5. Range history of Scenarios 1, 3, and 2 (top-down order) at (a) $Q_0 = 80\,\mathrm{Ah}$ and (b) $Q_0 = 69.3\,\mathrm{Ah}$.

tained below 50% of its capacity. Second, we focus on which battery type gives the most number of cycles (distance) for each velocity instead of operating at the optimal velocity. Lastly, we fix the flight distance (50 km) and increase the battery DOD to maintain it over the battery life, which increases the decay curve slopes in a similar manner described in Eq. (14) by multiplying $\mathrm{DOD_{now}}/\mathrm{DOD_{initial}}$.

In Fig. 6(a), it is advisable to choose a battery with the square-root degradation (Scenario 2) for velocities below 146 km/h. At this velocity, three scenarios achieve the almost identical performance (7000 cycles $\times$ 50 km/cycle $=$ 3.5×10^5 km), so the electric aircraft designer need not worry about the battery choices at the cost of reduced ranges. Figure 6(b) depicts the battery DOD history of each scenario at 146 km/h. Beyond this velocity, Scenario 1 (linear) is predominant. This example demonstrates the utility of integrating battery degradation into electric flight missions.

5. Conclusion

In light of the growing interest in electric flight, this work, for the first time, applied several battery degradation scenarios to evaluate the long-term performance of electric aircraft. Three battery-aging scenarios were considered which have linear, square-root, and exponential decay patterns. Unlike endurance, flight range was affected significantly by battery degradation patterns. The mechanism behind this phenomenon was investigated via a virtual full-discharge mission first. Those battery-decaying patterns were then ranked using a more realistic mission profile. The follow-up work should focus on incorporating the operational costs to quantify the economic impact of battery choices in electric aircraft using field data (e.g., air taxis).

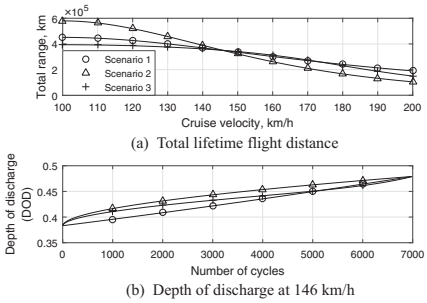

(a) Total lifetime flight distance

(b) Depth of discharge at 146 km/h

Fig. 6. Sample UAM-like mission (50 km flight leg).

Acknowledgments

The authors appreciate helpful contributions from Prof. Olivier de Weck and constructive comments from reviewers.

References

1) Uber Elevate: Fast-Forwarding to a Future of On-Demand Urban Air Transportation, 2018, https://www.uber.com/elevate.pdf (accessed September 20, 2018).
2) Sun, X., Wandelt, S., and Stumpf, E.: Competitiveness of On-demand Air Taxis Regarding Door-to-door Travel Time: A Race through Europe, *Transp. Res. E Logist. Transp. Rev.*, **119** (2018), pp. 1–18.
3) Paek, S. W., Kim, S., and Raj, R. V.: Impact of Battery Degradation on Lifetime Ranges of Electric Aircraft and Unmanned Underwater Vehicles, 2019 IEEE Conference on Control Technology and Applications, 2019, pp. 79–85.
4) Traub, L. W.: Range and Endurance Estimates for Battery-Powered Aircraft, *J. Aircraft*, **48** (2011), pp. 703–707.
5) Kaptsov, M. and Rodrigues, L.: Flight Management Systems for All-Electric Aircraft, 2017 IEEE Conference on Control Technology and Applications (CCTA), Hawaii, 2017, pp. 2126–2131.
6) Kaptsov, M. and Rodrigues, L.: Electric Aircraft Flight Management Systems: Economic Mode and Maximum Endurance, *J. Guid. Control Dynam.*, **41** (2018), pp. 285–290.
7) Wang, A., Kadam, S., Li, H., Shi, S., and Qi, Y.: Review on Modeling of the Anode Solid Electrolyte Interphase (SEI) for Lithium-ion Batteries, *NPJ Comput. Mater.*, **4** (2018), pp. 1–26.
8) Jouin, M., Bressel, M., Morando, S., Gouriveau, R., Hissel, D., Péra, M.-C., Zerhouni, N., Jemei, S., Hilairet, M., and Bouamama, B.: Estimating the End-of-life of PEM Fuel Cells: Guidelines and Metrics, *Appl. Mater.*, **177** (2016), pp. 87–97.
9) Petzl, M., Kasper, M., and Danzer, M. A.: Lithium Plating in a Commercial Lithium-ion Battery—A Low-temperature Aging Study, *J. Power Sources*, **275** (2015), pp. 799–807.
10) Anderson, J.: *Aircraft Performance and Design*, McGraw-Hill, New York, 1999.
11) Kokam Li-Ion/Polymer Cell, http://kokam.com/wp-content/uploads/2016/03/SLPB-Cell-Brochure.pdf (accessed August 25, 2019).
12) Spotniz, R.: Simulation of Capacity Fade in Lithium-ion Batteries, *J. Power Sources*, **113** (2003), pp. 72–80.
13) Smith, K., Saxon, A., Keyser, M., Lundstrom, B., Cao, A., and Roc, A.: Life Prediction Model for Grid-connected Li-ion Battery Energy Storage, 2017 American Control Conference, Seattle, USA, 2017, pp. 1–7.
14) Ploehn, H. J., Ramadass, P., and White, R. E.: Solvent Diffusion Model for Aging of Lithium-Ion Battery Cells, *J. Electrochem. Soc.*, **151** (2004), pp. A456–A462.

Keumjin Lee
Associate Editor